

Optical Characterization of Europium-doped Indium Hydroxide Nanocubes Obtained by Microwave-Assisted Hydrothermal Method

Fabiana Villela da Motta^{a*}, Ana Paula de Azevedo Marques^b, Vinícius Dantas de Araújo^a,
Mara Tatiane de Souza Tavares^a, Mauricio Roberto Bomio Delmonte^a, Carlos Alberto Paskocimas^a,
Máximo Siu Li^c, Rubens Maribondo do Nascimento^a, Elson Longo^d

^aDepartamento de Engenharia de Materiais – DEMAT, Centro de Tecnologia – CT, Universidade Federal do Rio Grande do Norte – UFRN, Av. Sen. Salgado Filho, 3000, CEP 59072-970, Natal, RN, Brazil

^bUniversidade Federal de São Paulo – UNIFESP, Rua Prof. Artur Riedel, 275, CEP 09972-270, Diadema, SP, Brasil

^cInstituto de Física de São Carlos – IFSC, Universidade de São Paulo – USP, Av. Trabalhador São Carlense, 400, CEP 13566-590, São Carlos, SP, Brazil

^dLaboratório Interdisciplinar de Eletroquímica e Cerâmica – LIEC, Instituto de Química – IQ, Universidade Estadual Paulista – UNESP, Rua Francisco Degni s/n, CEP 14801-907, Araraquara, SP, Brazil

Received: November 25, 2013; Revised: April 6, 2014

Crystalline europium-doped indium hydroxide (In(OH)₃:Eu) nanostructures were prepared by rapid and efficient Microwave-Assisted Hydrothermal (MAH) method. Nanostructures were obtained at low temperature. FE-SEM images confirm that these samples are composed of 3D nanostructures. XRD, optical diffuse reflectance and photoluminescence (PL) measurements were used to characterize the products. Emission spectra of europium-doped indium hydroxide (IH:xEu) samples under excitation (350.7 nm) presented broad band emission regarding the indium hydroxide (IH) matrix and ⁵D₀ → ⁷F₀, ⁵D₀ → ⁷F₁, ⁵D₀ → ⁷F₂, ⁵D₀ → ⁷F₃ and ⁵D₀ → ⁷F₄ europium transitions at 582, 596, 618, 653 and 701 nm, respectively. Relative intensities of Eu³⁺ emissions increased as the concentration of this ion increased from 0, 1, 2, 4 and 8 mol %, of Eu³⁺, but the luminescence is drastically quenched for the IH matrix.

Keywords: indium hydroxide, europium, Microwave-Assisted Hydrothermal, nanostructures

1. Introduction

Self-assembled micro-, meso- and nanostructures with specific morphology, novel properties and wide application potential in many fields are of great interest to chemists and material scientists due to their fundamental significance for addressing some basic issues of the quantum confinement effect and space-confined transport phenomena as well as their potential applications as advanced materials in functional nanodevices¹.

Indium hydroxides, oxyhydroxides, and oxides are important semiconductor materials, which have attracted much attention in the past decade. Cubic In(OH)₃, orthorhombic InOOH, and cubic and hexagonal In₂O₃ are their common phases². In(OH)₃ is a wide-gap semiconductor with Eg = 5.15 eV, with applications as a photocatalyst, among others³⁻⁵. InOOH (Eg = 3.5 eV) is also a typical wide-gap semiconductor⁶. Both cubic and hexagonal In₂O₃ are good n-type semiconductors with band gaps of 3.55-3.75 eV (which is close to that of GaN), which have been widely used as solar cells⁷, transparent conductors⁸, and sensors².

Regarding indium hydroxide (IH), Shi et al.⁹ recently reported a IH truncated polyhedral microcrystal formation via conventional hydrothermal treatment at 180°C for 16 h and 18 h that showed PL spectrum with two emission peaks at 496.6 and 419.2 nm using excitation wavelength (380 nm at room temperature). Yan et al.⁴ showed a broad band PL blue-green emission peak of IH nanocubes centered at 480 nm.

Rare earth ions such as Eu³⁺ can be added to semiconductors to increase PL. Europium in its trivalent state is one of the most studied among rare earth ions by luminescence spectroscopy due to the simplicity of its spectra and wide application as red phosphor in color TV screens. This ion has also attracted significant research attention due to its potential application as biological sensors, phosphors, electroluminescent devices, optical amplifiers or lasers when used as doping in a variety of materials^{10,11}. Dutta et al.¹² showed Eu³⁺ and Dy³⁺ doped indium oxide nanoparticles synthesized by a sonochemical technique. Eu³⁺ transitions were observed after excitation at 235 nm which is possibly due to the highly strained and

*e-mail: fabiana@ct.ufrn.br

distorted environment around Eu^{3+} ions in the In_2O_3 lattice matrix.

Indium hydroxides with different morphology such as spheres¹³, flowers^{14,15}, cubes¹⁶⁻²², rods^{23,24}, etc., have been synthesized by several synthesis methods. The physical and chemical properties of these powders can be influenced by particle shape and size distribution, which depend on the synthesis method. Conventional hydrothermal synthesis has been used to obtain IH structures using a simple, practical and environmentally friendly method^{4,13,18}.

Komarneni et al.²⁵ proposed the use of microwave radiation in the hydrothermal system by promoting the development of a new technique offering reaction kinetic enhancement, formation of materials with different morphology, low synthesis temperature and reduced processing times. Recently, Microwave-Assisted Hydrothermal (MAH) method was successfully used to obtain IH^[21] and other oxides such as ZnO ^[26,27], BaTiO_3 ^[28], CuO ^[29], SrMoO_4 ^[30], CeO_2 ^[31] and BaMoO_4 ^[32].

In previous publications^{17,33}, the synthesis and characterization of efficient luminescent indium hydroxides nanostructures, pure and doped with Tb^{3+} , was described and it was verified that these materials are highly promising candidates for electronic and optical applications. Thus, studies on the effect of different rare earth dopants, such as Eu^{3+} , on the synthesis and optical properties of indium hydroxide nanostructures synthesized by the MAH method are required to improve the scientific knowledge regarding future photoluminescent applications.

In this paper, we report the synthesis of $\text{In}(\text{OH})_3:\text{Eu}$ (IH: $x\text{Eu}$) nanostructures with concentrations of $x = 0, 1, 2, 4$ and $8 \text{ mol } \%$ of Eu^{3+} using the MAH method at a low temperature of 140°C for 30 min. IH:Eu nanoarchitectures, the morphology and PL properties of these samples were investigated.

2. Experimental Procedures

Using the previously reported MAH method³³, $\text{In}(\text{OH})_3:\text{Eu}$ (IH: $x\text{Eu}$) powders were obtained. About 3.6 Mmol of Indium (III) chloride (99% purity, Aldrich) and europium nitrate were dissolved in 80 mL of deionized water under constant stirring. Europium nitrate reagent was obtained by adding nitric acid to europium (III) oxide (Aldrich, USA, 99.999%) at 70°C . Eu^{3+} ion was added in the following percentages: 0, 1, 2, 4 and 8 mol %. The solution pH was adjusted to 10 by adding NH_4OH . After stirring for 10 min, 1 mL of polyethyleneglycol PEG (M_w 600) was added to the solution, and the mixture was then transferred to a Teflon autoclave. The system was sealed and placed in domestic microwave oven (2.45 GHz, maximum power of 800 W). The reaction system was heat treated at 140°C for 30 min (heating rate fixed at $25^\circ\text{C}/\text{min}$).

After MAH treatment, the white precipitate was washed with distilled water and dried at room temperature. The powders were characterized by X-ray diffraction (XRD) using Rigaku diffractometer (Model D/max-2500/PC) with $\text{Cu K}\alpha$ radiation. IH morphology and size were observed by field emission scanning electron microscopy (FE-SEM; Jeol JSM 6330F) images. UV-Vis reflectance spectra of IH powders were taken using Cary 5G equipment. PL spectra

were measured using Thermal Jarrel-Ash Monospec 27 monochromator and Hamamatsu R446 photomultiplier. The 350.7 nm line of a krypton ion laser (Coherent Innova 90 K) was used as the excitation source with output power of lasers kept at 200 mW. All measurements were taken at room temperature.

3. Results and Discussion

The X-ray patterns of IH powders synthesized with different Eu^{3+} percentages at 140°C are presented in Figure 1a-e. Figure 1a shows that all diffraction peaks could be indexed to the cubic lattice [space group $Im\bar{3}(204)$] to pure IH. With europium percentage increments (Figure 1b-e), the phases obtained by MAH treatment were basically IH with cubic structure (JCPDS card No. 16-0161) and the second phase in the InOOH formation with orthorhombic structure was observed [space group $P21nm(31)$] (JCPDS card No.71-2283).

The synthesis of IH and InOOH nanostructures is based on reactions (1 and 2)³⁴. Chen et al.³⁵ reported that the InOOH phase and the morphology synthesized by ultrasound-assisted solvothermal route can be controlled by the choice of the alkaline media and also the solvent. The factors reported for the formation of InOOH hollow spheres synthesized by conventional hydrothermal method were temperature treatment, reaction time, reagents and solution pH^{6,36}. We believe that the synthesis conditions are influenced by the use of europium nitrate as a source of Eu^{3+} . The pH value of solutions decreased with increases in the europium nitrate concentration; therefore, larger amounts of NH_4OH were used to obtain pH = 10, thus favoring the InOOH formation.



To the best of our knowledge, the optical properties of IH:Eu have rarely been studied. Figure 2 shows the PL spectra of IH: $x\text{Eu}$ cube-like structures at room temperature. Efficient red emission can be observed when this matrix is doped with Eu^{3+} , showing potential application for nanoarchitectures to serve as efficient red phosphor in luminescent nanodevices. Much effort has been dedicated to the study of PL in nanostructural materials since the first visible PL at room temperature was observed in porous silicon for the first time³⁷. Rare ions are used to dope oxides not only as a probe to investigate local centers and energy³⁸⁻⁴⁰, but also to provoke changes in the optical behavior.

Optical diffuse reflectance measurements have been carried out on IH: $x\text{Eu}$ particles obtained under MAH conditions. An estimation of the optical band gap " E_{gap} " (Table 1) was obtained using the Wood & Tauc method⁴¹. The calculated E_{gap} values were 5.12, 4.88, 3.63, 3.56 and 3.55 eV for samples treated at 140°C for 30 min, pure and with 1, 2, 4 and 8 mol % Eu^{3+} , respectively. The E_{gap} reduction with increasing Eu^{3+} content can be associated with the formation of the InOOH phase. Zhu et al.⁶ studied InOOH hollow spheres synthesized by conventional hydrothermal method

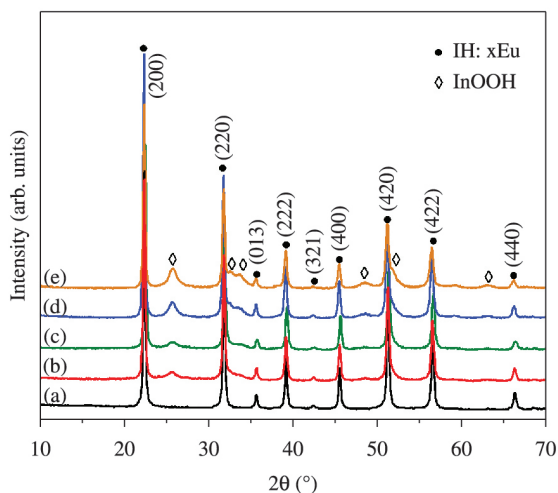


Figure 1. XRD patterns of IH:xEu powders obtained by the MAH method at 140°C for 30 min: (a) $x = 0$, (b) $x = 1$, (c) $x = 2$, (d) $x = 4$ and (e) $x = 8$ mol %.

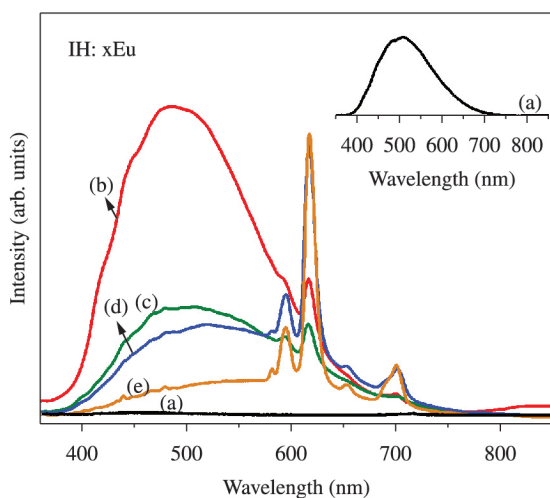


Figure 2. PL spectra of IH:xEu structures obtained by the MAH method at 140°C for 30 min: (a) $x = 0$, (b) $x = 1$, (c) $x = 2$, (d) $x = 4$ and (e) $x = 8$ mol %.

Table 1. Optical band gap (E_{gap}) and fitting parameters of the Gaussian peaks for PL of the IH matrix obtained with excitation wavelength at 350.7 nm.

| IH:xEu | E_{gap} (eV) | Peak center (nm) | | | |
|---------|-----------------------|------------------|----------------|----------------|----------------|
| | | 450 | 512 | 570 | 623 |
| | | % ^a | % ^a | % ^a | % ^a |
| $x = 0$ | 5.12 | 18 | 55 | 13 | 14 |
| $x = 1$ | 4.88 | 29 | 49 | 14 | 8 |
| $x = 2$ | 3.63 | 25 | 31 | 26 | 18 |
| $x = 4$ | 3.56 | 21 | 19 | 27 | 33 |
| $x = 8$ | 3.55 | 11 | 18 | 39 | 32 |

^aPercentage obtained by dividing the area of each decomposed PL curves by the total PL area.

and estimated that the optical band gap was 3.5eV and the E_{gap} value for crystalline $\text{In}(\text{OH})_3$ powders was 5.15 eV^[5]. Pure IH or IH:Eu belongs to n-type semi-conductors where oxygen vacancies can induce the formation of new energy levels in the band gap. The generation of oxygen defects in the crystalline structure of cube-like crystals of pure IH and IH:Eu are apparent. The formation of InOOH during synthesis for samples with europium releases molecular water (reaction 2) and provides oxygen vacancies in the lattice. Thus, during the MAH process, the displacement of oxygen related to In or Eu modulates different species of trapped holes (V_o^\bullet ; $V_o^{\bullet x}$ and $V_o^{\bullet\bullet}$ species) around $[\text{InO}_5 V_o^x]$ clusters and gives rise to complex cluster vacancies^[6].

Emission spectra in Figure 2 were obtained under excitation of 350.7nm. The efficient sharp peak is attributed to ${}^5D_0 \rightarrow {}^7F_1$ emission transition, indicating the presence of Eu^{3+} ion in the IH lattice. Emission spectra of IH:Eu structures exhibit an efficient red PL emission peak centered at around 618 nm, corresponding to the forced electric dipole transition ${}^5D_0 \rightarrow {}^7F_2$ which is allowed in this particular case since europium does not occupy a symmetry center in the indium hydroxide. Another weaker emission at ${}^5D_0 \rightarrow {}^7F_0$, ${}^5D_0 \rightarrow {}^7F_1$, ${}^5D_0 \rightarrow {}^7F_3$ and ${}^5D_0 \rightarrow {}^7F_4$ corresponding to Eu^{3+} transitions can be observed at around 582, 596, 653 and 701 nm, respectively^[42,43].

The relative intensities of Eu^{3+} emissions increase as the concentration of this ion increases from 1 to 8 mol %; however the luminescent emission of the IH matrix is drastically quenched. When the Eu^{3+} concentration is higher, the mechanism that prevails is the energy transfer from the IH matrix to Eu^{3+} . This energy migration process is responsible for the increase in Eu^{3+} luminescence^[43,44].

For Eu-doped inorganic materials, optical transitions occur mainly from 5D_0 to 7F_J ($0 < J < 6$) manifold, giving rise to a series of red emission lines with intensities depending on the local Eu^{3+} environment. From all possible transitions, only ${}^5D_0 \rightarrow {}^7F_1$ is magnetically dipole allowed in the free ion; all others require J-level mixing induced by the crystal field. Whereas the odd-parity components of the crystal field enable electric dipole transitions between 5D_0 and ${}^7F_{2,4,6}$ in the first order, a combination of odd and even crystal-field terms gives rise to faint second-order transitions for the remaining $J = 0, 3, 5$ values. The intensities of the different J transitions, and in particular the hypersensitive $J = 2$ peak provide a good measure of the local crystal field acting on Eu^{3+} ions^[45].

Assuming the PL emission peaks can be described with a Gaussian function, the emission envelope in Figure 2 can be fitted to multiple peaks (Figure 3a-e). In the emission envelope from IH:xEu, each color represents a different type of electronic transition and can be linked to a specific structural arrangement^[46]. To better understanding PL properties, the curves were analyzed using the PeakFit deconvolution software^[47]. Based on the Gaussian line broadening mechanism for luminescence processes, the fine features in the PL spectra of the IH matrix were deconvoluted and extracted from deconvolution curves. Figure 3a-e illustrates such decompositions while Table 1 lists the areas under the curve of the respective transitions.

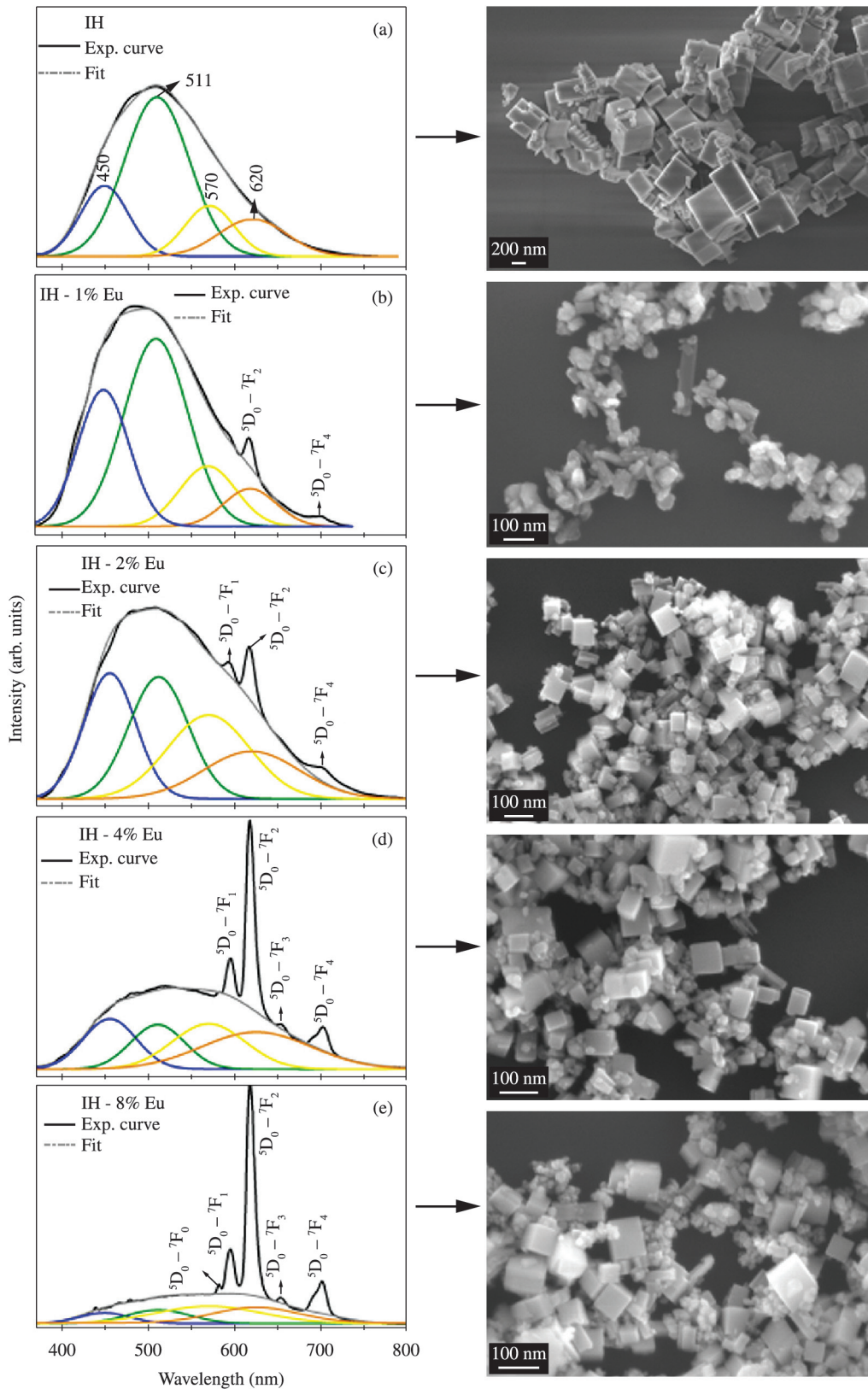


Figure 3. Deconvolution of a PL curve fitted for IH:xEu samples and respective Fe-SEM images (on the side): (a) $x = 0$, (b) $x = 1$, (c) $x = 2$, (d) $x = 4$ and (e) $x = 8$ mol %..

The IH matrix PL curves for all samples are composed of four PL components with the following maxima nm: blue = 450 nm, green = 512 nm, yellow = 570 nm and orange = 623 nm. The PL deconvolution shows the IH matrix ordered-to- disordered structure changing with the increase percentage in the Eu^{3+} ion which favors yellow and orange light emission (higher wavelength) for smaller energies. According to the calculated band gap values (E_{gap}), the increase percentage in the Eu^{3+} ion decreased the E_{gap} value and therefore increased the short-range disorder for clusters in the matrix. The appropriate structural disorder can result in better PL emission as compared with a completely ordered emission. Structurally disordered materials in general present oxygen vacancies, lattice defects, impurities and/or local bond distortions which yield localized electronic levels in their band gap⁴³. Figure 3a-e (on the side) depicts FE-SEM images of IH:xEu nanostructures obtained at 140°C for 30 min. Figure 3a shows cubic and irregularly-shaped structures of pure IH with smooth and uniform surface where the angle between adjacent edges is relatively close to 90°; however, differences in the morphology of IH to IH:1%Eu were apparent. In sample with 1% Eu the

formation of a well-defined cube-like structure and a slight decrease were observed. It is speculated that europium at this concentration (1%) promotes disorder in the IH matrix. This characteristic can be confirmed with an increase in the PL property observed in IH:1%Eu as compared with the IH matrix. The increase in the europium concentration from 2% to 8% Eu promotes reorganization of the system and an increase in the cube-like structure is again observed. A decrease in the IH matrix PL property was observed with an increase in the europium concentration, suggesting that the order in the system increases.

4. Conclusions

IH:xEu powders (where x=0, 1, 2, 4 and 8 mol %) were efficiently obtained in their crystalline phase using the MAH method at 140°C for 30 min. The relative intensities of Eu^{3+} ion emissions increase as the concentration of this ion increases from 1 to 8 mol % while in the IH matrix sample the luminescence intensity was drastically quenched. The mechanism that prevails in this case is the energy transfer from the IH matrix to Eu^{3+} . These optical properties

exhibited by IH:xEu suggest that this material is a highly promising candidate for photoluminescent applications.

Acknowledgements

The authors thank the financial support of the Brazilian research financing institutions: FAPESP-CDMF 2013/07296-2, CNPq and CAPES. In memory of M. F. C. Abreu.

References

- Cao AM, Hu JS, Liang HP and Wan LJ. Self-assembled vanadium pentoxide (V_2O_5) hollow microspheres from nanorods and their application in lithium-ion batteries. *Angewandte Chemie*. 2005; 44(28):4391-4395. PMID:15942965. <http://dx.doi.org/10.1002/anie.200500946>
- Zhuang Z, Peng Q, Liu J, Wang X and Li Y. Indium hydroxides, oxyhydroxides, and oxides nanocrystals series. *Inorganic Chemistry*. 2007; 46(13):5179-5187. PMID:17530840. <http://dx.doi.org/10.1021/ic061999f>
- Lei ZB, Ma GL, Liu MY, You WS, Yan HJ, Wu GP et al. Sulfur-substituted and zinc-doped $\text{In}(\text{OH})_3$: a new class of catalyst for photocatalytic H_2 production from water under visible light illumination. *Journal of Catalysis*. 2006; 237(2):322-329. <http://dx.doi.org/10.1016/j.jcat.2005.11.022>
- Yan T, Wang X, Long J, Liu P, Fu X, Zhang G et al. Urea-based hydrothermal growth, optical and photocatalytic properties of single-crystal line $\text{In}(\text{OH})_3$ nanocubes. *Journal of Colloid and Interface Science*. 2008; 325(2):425-431. PMID:18555265. <http://dx.doi.org/10.1016/j.jcis.2008.05.065>
- Avivi S, Mastai Y and Gedanken A. Sonochemical synthesis of In^{3+} ions: formation of needlelike particles of indium hydroxide. *Chemistry of Materials*. 2000; 12(5):1229-1233. <http://dx.doi.org/10.1021/cm9903677>
- Zhu HL, Yao KH, Zhang H and Yang DR. In OOH hollow spheres synthesized by a simple hydrothermal reaction. *Journal of Physical Chemistry B*. 2005; 109(44):20676-20679. PMID:16853679. <http://dx.doi.org/10.1021/jp0511911>
- Katoh R, Furube A, Yoshihara T, Hara K, Fujihashi G, Takano S et al. Efficiencies of electron injection from excited N_3 dye into nanocrystalline semiconductor (ZrO_2 , TiO_2 , ZnO , Nb_2O_5 , SnO_2 , In_2O_3) films. *Journal of Physical Chemistry B*. 2004; 108(15):4818-4822. <http://dx.doi.org/10.1021/jp031260g>
- Kim H, Horwitz JS, Kushto GP, Qadri SB, Kafafi ZH and Chrisey DB. Transparent conducting Zr-doped In_2O_3 thin films for organic light-emitting diodes. *Applied Physics Letters*. 2001; 78(8):1050-1052. <http://dx.doi.org/10.1063/1.1350595>
- Shi Z, Wang W and Zhang Z. Synthesis and characterization of indium hydroxide truncated polyhedral microcrystals. *Materials Letters*. 2008; 62(27):4293-4295. <http://dx.doi.org/10.1016/j.matlet.2008.07.006>
- Silva CC, Filho FP, Sombra ASB, Rosa ILV, Leite ER, Longo E et al. Study of structural and photoluminescent properties of $\text{Ca}_8\text{Eu}_2(\text{PO}_4)_6\text{O}_2$. *Journal of Fluorescence*. 2008; 18(2):253-259. PMID:18049883. <http://dx.doi.org/10.1007/s10895-007-0242-9>
- Morais EA, Scalvi LVA, Tabata A, Oliveira JBB and Ribeiro SJL. Photoluminescence of Eu^{3+} ion in SnO_2 obtained by sol-gel. *Journal of Materials Science*. 2008; 43(1):345-349. <http://dx.doi.org/10.1007/s10853-007-1610-1>
- Dutta DP, Sudarsan V, Srinivasu P, Vinu A and Tyagi AK. Indium oxide and europium/dysprosium doped indium oxide nanoparticles: Sonochemical synthesis, characterization, and photoluminescence studies. *Journal of Physical Chemistry C*. 2008; 112(17):6781-6785. <http://dx.doi.org/10.1021/jp800576y>
- Li B, Xie Y, Jing M, Rong G, Tang Y and Zhang G. In_2O_3 hollow microspheres: synthesis from designed in (OH)(3) precursors and applications in gas sensors and photocatalysis. *Langmuir*. 2006; 22(22):9380-9385. PMID:17042557. <http://dx.doi.org/10.1021/la061844k>

14. Zhu H, Wang X, Wang Z, Yang C, Yang F and Yang X. Self-assembled 3D microflowerly In(OH)(3) architecture and its conversion to In₂O₃. *Journal of Physical Chemistry C*. 2008; 112(39):15285-15292. <http://dx.doi.org/10.1021/jp804768w>
15. Zhu H, Wang X, Yang F and Yang X. Template-free, surfactantless route to fabricate In(OH)₃ monocrystalline nanoarchitectures and their conversion to In₂O₃. *Crystal Growth & Design*. 2008; 8(3):950-956. <http://dx.doi.org/10.1021/cg700850e>
16. Motta FV, Lima RC, Marques APA, Leite ER, Varela JA and Longo E. In₂O₃ microcrystals obtained from rapid calcination in domestic microwave oven. *Materials Research Bulletin*. 2010; 45(11):1703-1706. <http://dx.doi.org/10.1016/j.materresbull.2010.06.056>
17. Motta FV, Lima RC, Marques APA, Li MS, Leite ER, Varela JA et al. Indium hydroxide nanocubes and microcubes obtained by microwave-assisted hydrothermal method. *Journal of Alloys and Compounds*. 2010; 497(1-2):L25-L28. <http://dx.doi.org/10.1016/j.jallcom.2010.03.069>
18. Zhu HL, Wang NY, Wang L, Yao KH and Shen XF. In situ x-ray diffraction study of the phase transition of nanocrystalline In(OH)₃ to In₂O₃. *Inorganic Materials*. 2005; 41(6):609-612. <http://dx.doi.org/10.1007/s10789-005-0178-x>
19. Tang Q, Zhou WJ, Zhang W, Ou SM, Jiang K, Yu WC et al. Size-controllable growth of single crystal In(OH)(3) and In₂O₃ nanocubes. *Crystal Growth & Design*. 2005; 5(1):147-150. <http://dx.doi.org/10.1021/cg049914d>
20. Zhu HL, Wang Y, Wang NY, Li Y and Yang J. Hydrothermal synthesis of indium hydroxide nanocubes. *Materials Letters*. 2004; 58(21):2631-2634. <http://dx.doi.org/10.1016/j.matlet.2004.03.030>
21. Koga N and Kimizu T. Thermal Decomposition of Indium(III) Hydroxide Prepared by the Microwave-Assisted Hydrothermal Method. *Journal of the American Ceramic Society*. 2008; 91(12):4052-4058. <http://dx.doi.org/10.1111/j.1551-2916.2008.02811.x>
22. Chen LY, Zhang YG, Wang WZ and Zhang ZD. Tunable synthesis of various hierarchical structures of In(OH)(3) and In₂O₃ assembled by nanocubes. *European Journal of Inorganic Chemistry*. 2008; (9):1445-1451. <http://dx.doi.org/10.1002/ejic.200700936>
23. Wang L, Perez-Maqueda LA and Matijevic E. Rapid preparation of uniform colloidal indium hydroxide by the controlled double jet precipitation. *Colloid and Polymer Science*. 1998; 276(9):847-850. <http://dx.doi.org/10.1007/s003960050320>
24. Perez-Maqueda LA, Wang LF and Matijevic E. Nanosize indium hydroxide by peptization of colloidal precipitates. *Langmuir*. 1998; 14(16):4397-4401. <http://dx.doi.org/10.1021/la980149c>
25. Komarneni S, Roy R and Li QH. Microwave-hydrothermal Synthesis of Ceramic Powders. *Materials Research Bulletin*. 1992; 27(12):1393-1405. [http://dx.doi.org/10.1016/0025-5408\(92\)90004-J](http://dx.doi.org/10.1016/0025-5408(92)90004-J)
26. Lima RC, Macario LR, Espinosa JWM, Longo VM, Erlo R, Marana NL et al. Toward an understanding of intermediate- and short-range defects in ZnO single crystals: a combined experimental and theoretical study. *Journal of Physical Chemistry A*. 2008; 112(38):8970-8978. PMID:18652436. <http://dx.doi.org/10.1021/jp8022474>
27. Milao TM, Mendonça VR, Araujo VD, Avansi W, Ribeiro C, Longo E et al. Microwave hydrothermal synthesis and photocatalytic performance of ZnO and M:ZnO nanostructures (M = V, Fe, Co). *Science of Advanced Materials*. 2012; 4(1):54-60. <http://dx.doi.org/10.1166/sam.2012.1251>
28. Moreira ML, Mambrini GP, Volanti DP, Leite ER, Orlandi MO, Pizani PS et al. Hydrothermal microwave: a new route to obtain photoluminescent crystalline BaTiO₃ nanoparticles. *Chemistry of Materials*. 2008; 20(16):5381-5387. <http://dx.doi.org/10.1021/cm801638d>
29. Volanti DP, Keyson D, Cavalcante LS, Simões AZ, Joya MR, Longo E et al. Synthesis and characterization of CuO flower-nanostructure processing by a domestic hydrothermal microwave. *Journal of Alloys and Compounds*. 2008; 459(1-2):537-542. <http://dx.doi.org/10.1016/j.jallcom.2007.05.023>
30. Sczancoski JC, Cavalcante LS, Joya MR, Varela JA, Pizani PS and Longo E. SrMoO₄ powders processed in microwave-hydrothermal: synthesis, characterization and optical properties. *Chemical Engineering Journal*. 2008; 140(1-3):632-637. <http://dx.doi.org/10.1016/j.cej.2008.01.015>
31. Araújo VD, Avansi W, Carvalho HB, Moreira ML, Longo E, Ribeiro C et al. CeO₂ nanoparticles synthesized by a microwave-assisted hydrothermal method: evolution from nanospheres to nanorods. *CrystEngComm*. 2012; 14(3):1150-1154. <http://dx.doi.org/10.1039/c1ce06188g>
32. Sczancoski JC, Cavalcante LS, Marana NL, Silva RO, Tranquilin RL, Joya MR et al. Electronic structure and optical properties of BaMoO₄ powders. *Current Applied Physics*. 2010; 10(2):614-624. <http://dx.doi.org/10.1016/j.cap.2009.08.006>
33. Motta FV, Marques APA, Li MS, Abreu MFC, Paskocimas CA, Bomio MRD et al. Preparation and photoluminescence characteristics of In(OH)₃:xTb³⁺ obtained by Microwave-Assisted Hydrothermal method. *Journal of Alloys and Compounds*. 2013; 553:338-342. <http://dx.doi.org/10.1016/j.jallcom.2012.11.063>
34. Xu X and Wang X. Size- and surface-determined transformations: from ultrathin InOOH nanowires to uniform c-In₂O₃ Nanocubes and rh-In₂O₃ nanowires. *Inorganic Chemistry*. 2009; 48(8):3890-3895. PMID:19326893. <http://dx.doi.org/10.1021/ic802449w>
35. Chen L, Ma X, Liu Y, Zhang YG, Wang W, Liang Y et al. 3D architectures of InOOH: ultrasonic-assisted synthesis, growth mechanism, and optical properties. *European Journal of Inorganic Chemistry*. 2007; (28):4508-4513. <http://dx.doi.org/10.1002/ejic.200700364>
36. Chen SG, Huang YF, Cheng Y, Xia Q, Liao HW and Long CG. Shape-controlled growth of In(OH)₃ crystals synthesized by diglycol-mediated solvothermal process. *Materials Letters*. 2008; 62(10-11):1634-1637. <http://dx.doi.org/10.1016/j.matlet.2007.09.048>
37. Canham LT. Silicon quantum wire array fabrication by electrochemical and chemical dissolution of wafers. *Applied Physics Letters*. 1990; 57(10):1046-1048. <http://dx.doi.org/10.1063/1.103561>
38. Xiong HM, Liu DP, Xia YY and Chen JS. Polyether-grafted ZnO nanoparticles with tunable and stable photoluminescence at room temperature. *Chemistry of Materials*. 2005; 17(12):3062-3064. <http://dx.doi.org/10.1021/cm050556r>
39. Fujihara S, Ogawa Y and Kasai A. Tunable visible photoluminescence from ZnO thin films through Mg-doping and annealing. *Chemistry of Materials*. 2004; 16(15):2965-2968. <http://dx.doi.org/10.1021/cm049599i>
40. Draeger EW, Grossman JC, Williamson AJ and Galli G. Optical properties of passivated silicon nanoclusters: The role of synthesis. *Journal of Chemical Physics*. 2004; 120(22):10807-10814. PMID:15268108. <http://dx.doi.org/10.1063/1.1738633>

41. Wood DL and Tauc J. Weak absorption tails in amorphous semiconductors. *Physical Review B*. 1972; 5(8):3144-3151. <http://dx.doi.org/10.1103/PhysRevB.5.3144>
42. Chong MK, Pita K and Kam CH. Photoluminescence of sol-gel-derived Y_2O_3 : Eu^{3+} thin-film phosphors with Mg^{2+} and Al^{3+} co-doping. *Applied Physics A: Materials Science & Processing*. 2004; 79(3):433-437. <http://dx.doi.org/10.1007/s00339-004-2737-4>
43. Rosa ILV, Marques APA, Tanaka MTS, Motta FV, Varela JA, Leite ER et al. Europium(III) Concentration effect on the spectroscopic and photoluminescent properties of $BaMoO_4$:Eu. *Journal of Fluorescence*. 2009; 19(3):495-500. PMID:19002571. <http://dx.doi.org/10.1007/s10895-008-0438-7>
44. Yu Y, Chen D, Wang Y, Huang P, Weng F and Niu M. Enhanced photoluminescence of Eu^{3+} induced by energy transfer from In_2O_3 nano-crystals embedded in glassy matrix. *Physical Chemistry Chemical Physics*. 2009; 11(39): 8774-8778. PMID:20449022. <http://dx.doi.org/10.1039/b907065f>
45. Stavale F, Pascua L, Nilius N and Freund HJ. From embedded nanoislands to thin films: Topographic and optical properties of europium oxide on $MgO(001)$ films. *Physical Review B*. 2012; 86(8). <http://dx.doi.org/10.1103/PhysRevB.86.085448>
46. Motta FV, Figueiredo AT, Longo VM, Mastelaro VR, Freitas AZ, Gomes L et al. Disorder-dependent photoluminescence in $Ba_{0.8}Ca_{0.2}TiO_3$ at room temperature. *Journal of Luminescence*. 2009; 129(7):686-690. <http://dx.doi.org/10.1016/j.jlumin.2009.01.014>
47. Ding T, Zheng WT, Tian HW, Zang JF, Zhao ZD, Yu SS et al. Temperature-dependent photoluminescence in $La_{2/3}Ca_{1/3}MnO_3$. *Solid State Communications*. 2004; 132(12):815-819. <http://dx.doi.org/10.1016/j.ssc.2004.09.047>